

# Model Tests on Seismic Performance of Retaining Walls

by

Yulman MUNAF<sup>1</sup>, Junichi KOSEKI<sup>2</sup>, Masaru TATEYAMA<sup>3</sup>,  
Kenichi KOJIMA<sup>4</sup>, Takeshi SATO<sup>5</sup>

## ABSTRACT

This paper is a preliminary report of ongoing studies for the purpose of developing a rational design method to evaluate stability for several types of conventional retaining walls during an earthquake. Since the seismic behavior of retaining walls is not yet completely understood, a series of tilting and shaking table tests on small scale model are performed. The observed failure pattern and critical condition are compared with the predicted ones that are calculated based on pseudo-static approach. The results show that they are qualitatively consistent. However, the angle of failure planes observed for shaking table tests is steeper than what is predicted. It may suggest that the seismic behavior assumed in the prediction is not fully correct.

## INTRODUCTION

The Hyogoken-Nambu Earthquake of January 17, 1995, caused serious damage to a number of conventional masonry and unreinforced concrete gravity type and leaning type retaining walls for railway embankments and also to many modern cantilever type retaining walls, while geogrid-reinforced soil retaining walls having a full height concrete facing performed very well (Tatsuoka et al.[1]). Back analyses of those retaining walls by pseudo-static limit equilibrium method have been made by Koseki et al.[2] in order to improve aseismic design procedures, where the potential failure mode was compared with the actual behavior, and the critical horizontal seismic coefficient that yields a safety factor of unity was compared with the estimated peak horizontal acceleration. However, their actual failure mechanism and seismic performance have not yet been fully understood. To this end, a series of tilting tests and shaking table tests for several models of retaining walls were performed.

## LATERAL EARTH PRESSURE

Lateral earth pressures that develop behind rigid retaining walls during seismic loading have been conventionally evaluated using a pseudo-static approach, which was introduced by Mononobe [3] and Okabe [4]. They proposed a modified Coulomb type analysis by adding inertia forces  $k_h W$  and  $k_v W$  to the soil wedge as shown in Fig. 1, in which  $W$  = the weight of soil contained within assumed failure wedge. The seismic coefficients  $k_h$  and  $k_v$  were defined as horizontal and vertical accelerations divided by gravity acceleration. Although this Mononobe-Okabe theory does not give the distribution of earth pressure, a hydrostatic type triangular distribution has been assumed similarly to that of the Rankine type static earth pressure.

---

1, 2, 5 : Institute of Industrial Science, Univ. of Tokyo

3, 4 : Railway Technical Research Institute

Based on the Mononobe-Okabe theory, the total force acting on the interface between the wall and the soil wedge is given by,

$$P_{ae} = 1/2 \cdot \gamma \cdot H^2 \cdot (1 - k_v) \cdot K_{ae}$$

where  $K_{ae}$  is an active earth pressure coefficient calculated by,

$$K_{ae} = \frac{\cos^2(\phi - \psi - \theta)}{\cos\theta \cdot \cos^2\psi \cdot \cos(\delta + \psi + \theta) \left[ 1 + \sqrt{\frac{\sin(\phi + \delta) \cdot \sin(\phi - \beta - \theta)}{\cos(\delta + \psi + \theta) \cdot \cos(\psi - \beta)}} \right]^2}$$

The angle of failure plane  $\xi$  is given by,

$$\cot(\xi - \beta) = -\tan(\phi + \delta + \psi - \beta) + \sec(\phi + \delta + \psi - \beta) \cdot \sqrt{\frac{\cos(\psi + \delta + \theta) \cdot \sin(\phi + \delta)}{\cos(\psi - \beta) \cdot \sin(\phi - \beta - \theta)}}$$

$$\theta = \tan^{-1} \frac{k_h}{1 - k_v}$$

$k_h$  = horizontal acceleration / g

$k_v$  = vertical acceleration / g

The Mononobe-Okabe theory is based on three fundamental assumptions (after Steedman and Zeng [5]);

1. The wall has already deformed outwards sufficiently to generate minimum active earth pressure.
2. A soil wedge, with a planar sliding surface running through the base of wall, is on the point of failure with maximum shear strength mobilized along the length of sliding surface.
3. The soil behind the wall behaves as a rigid body so that accelerations can be assumed to be uniform throughout the backfill at the instant of failure.

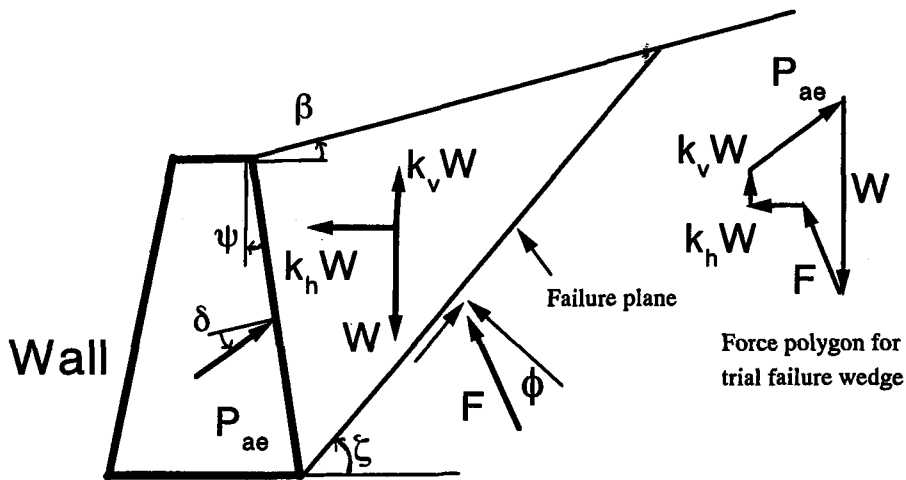


Fig. 1 Schematic Forces Acting on Soil Wedge Assumed in Mononobe-Okabe Theory

Several researchers followed this theory to propose modified design methods of gravity retaining walls based on limit permanent displacement concept (e.g., Richards and Elms [6] and Whitman and Liao [7]).

## MODEL OF RETAINING WALLS

### Design and Evaluation of Stability

Fig.2 shows the cross sections of retaining wall models which were used in this study. Their seismic stability was predicted based on procedures commonly used in design of actual retaining walls. The horizontal seismic coefficient  $k_h$  was considered to act at the center of gravity of retaining walls, and seismic earth pressures were calculated by the Mononobe-Okabe theory. The factor of safety against sliding and overturning failure were calculated using design parameters as shown in Table 1. The internal friction angle  $\phi$  of the sand was evaluated based on previous plane strain compression tests (Yoshida [8]), while the friction angle  $\delta_{wall}$  was varied between  $0-\phi$ . For overturning stability, the center of rotation was assumed at the toe of the wall base. Figs. 3 and 4 show typical safety factors plotted against tilting angle  $\theta$  for tilting tests and horizontal acceleration  $a$  for shaking table tests. From those figures the predicted critical angle  $\theta_{cr}$  and the predicted critical acceleration  $a_{cr}$  which yield safety factor equal to 1 were evaluated.

### Model Walls and Backfill Material

Fig. 5 shows a model wall used as the cantilever type. Facing and base parts of the wall were made of wooden block, which were reinforced with steel bar ( $\phi = 10$  mm) in vertical direction and metal plate in perpendicular direction. Their surfaces were covered with sand paper. To adjust the dead load, extra weights were added nearly at the center of gravity the model wall. To measure normal stress  $\sigma$  and shear stress  $\tau$  acting on the facing and to reduce the side wall friction effect, several units of two-component load cells were installed at the center part of the facing and base which contact with sand. Three displacement transducers were set at the facing and one at the base to measure rotation and displacement of walls. Toyoura sand was used as backfill and subsoil layers, which has  $e_{max} = 0.997$ ;  $e_{min} = 0.605$ ;  $G_s = 2.64$ ;  $D_{10} = 0.11$  mm and  $D_{50} = 0.16$  mm.

## TESTING PROCEDURES

### Tilting Tests

Testing procedures for tilting tests consist of 2 steps; (1) filling of sand; (2) tilting of sand box. Fig. 6 shows schematic diagram of these steps. The walls were free to slide and rotate during these steps. Air dried Toyoura sand was pluviated from the slit of hopper into a sand box 180 cm long, 86 cm high and 60 cm wide. The height of hopper from the sand surface was kept always constant. The opening of slit and traveling speed of the hopper were carefully controlled so as to obtain a uniform sand layer. To observe the failure pattern, horizontal layers at a thickness of 1 cm was prepared by using dyed Toyoura sand along the side walls and at the center of sand layer. On subsoil layers which was 20 cm thick, the retaining wall models were carefully installed, and back filling of sand was continued until the top layer

was complete. After trimming the surface of the top layer to the prescribed horizontal geometry, a surcharge by using lead shots was placed, and then the whole sand box was tilted until formation of failure plane was observed. At this point, the observed critical angle  $\theta_{cr}$  and the observed failure pattern was determined. During these processes, earth pressure acting on the retaining wall and displacements of the wall were measured.

### Shaking Table Tests

Similarly to the tilting tests, testing procedures for shaking table test consist of 2 steps; (1) filling of sand; (2) shaking of whole sand box. Fig. 7 shows schematic diagram of experimental set-up. A sand box 260 cm long, 140 cm high and 60 cm wide was used. To reduce effects of reflection by end walls of the box during shaking, the length of the backfill sand layers was extended to 150 cm (about 60 cm longer than that for tilting tests). Filling of sand to sand box was made similarly to the tilting tests. After filling of sand, the whole sand box was shaken using sinusoidal waves at a frequency of 5 Hz. Their amplitude was initially adjusted to give the desired base accelerations of 25 or 50 gals and was increased at an increment of 25 or 50 gal until formation of failure plane was observed. At this point, the observed critical acceleration  $a_{cr,obs.}$  and the observed failure pattern were determined. In addition to the measurement of earth pressures acting on the retaining wall and displacements of the wall, response accelerations of the wall and the backfill sand were recorded during the shaking.

## RESULTS AND DISCUSSIONS

### Tilting Tests

#### Failure Pattern

Observed failure plane and displacement of retaining walls are schematically shown in Fig.2. Two failure planes were observed for each test. One was inclined with an angle  $\zeta$ , which passed through the heel of base. The other was nearly vertical passing through the heel of base for cantilever type, and was at the interface between the facing and the backfill for leaning and gravity type. Table 2 summarizes the observed major failure pattern and the predicted critical angle  $\theta_{cr}$  which yields safety factors equal to 1. The predicted critical angle against overturning was smaller than that for sliding. This condition was consistent with the observation as shown in Table 2. In some tests, failure occurred at second tilting, possibly due to cyclic softening of the sand layer beneath the toe of the wall. Fig. 8 shows the angle of failure plane  $\zeta$  observed along the center line of the sand layer plotted against tilting angle  $\theta$ , which was nearly close to the predicted value at  $\delta_{wall}$  between  $1/2\phi$ -  $2/3\phi$ . Figs. 9 and 10 show ratio of predicted and observed critical angle  $\theta_{cr,pre.}/\theta_{cr,obs.}$  against overturning and sliding. The mobilized friction angle  $\delta_{wall}$  yielding  $\theta_{cr,pre.}/\theta_{cr,obs.}$  equal to 1 against overturning was between  $16.8^\circ$  and  $28.5^\circ$ , which was almost equal to or smaller than the aforementioned value based on the angle of failure plane. At this mobilized  $\delta_{wall}$ , the value of  $\theta_{cr,pre.}/\theta_{cr,obs.}$  against sliding was larger than 1 and was smallest for the leaning type among others as shown in Fig. 10.

## Earth Pressure

The observed lateral earth pressure acting on the facing increased monotonically due to increase of tilting angle. Fig.11 shows the distribution of the observed normal pressure  $\sigma$  plotted against depth for cantilever type. Before surcharge, the observed distribution was nearly triangular. However, after surcharge and during tilting of sand box, the normal pressures at upper part increased largely compared to those at lower part, due possibly to effects of the friction on the upper surface of the wall base. Fig. 12 shows the mobilized wall friction angle  $\delta_{wall}$  ( $= \tan^{-1} \tau/\sigma$ , where  $\tau$  is the observed shear stress acting on the facing) plotted against tilting angle  $\theta$ . The values of  $\delta_{wall}$  were not the same along the facing but were kept constant during tilting. Fig. 13 shows normal pressures acting on the bottom of wall base during tilting. At the toe of base, the increments of normal pressure was much larger than at the heel, which may suggest that the sand beneath the toe will fail at first, and overturning will occur around a rotational point near the toe. This condition was consistent with the observed failure pattern.

## Shaking Table Tests

### Failure Pattern

Table 3 shows the predicted critical acceleration  $a_{cr}$  and the observed major failure pattern. The predicted critical acceleration against overturning was smaller than against sliding. Photo 1 shows the failure patterns observed during shaking, which were similar to those observed during tilting tests. Fig. 14 shows the angle of observed failure plane along the center line of the sand layer plotted against input acceleration. The observed failure plane was steeper than the predicted ones. This behavior was different from tilting tests. Figs. 15 and 16 show the ratio of the predicted and the observed critical acceleration  $a_{cr,pre}/a_{cr,obs}$  against overturning and sliding. The mobilized friction angle  $\delta_{wall}$  yielding  $a_{cr,pre}/a_{cr,obs}$  equal to 1 against overturning was between  $24.4^\circ$  and  $27.9^\circ$ , which was consistent with the corresponding value by tilting test for cantilever type and gravity type as shown in Fig. 9. At this mobilized angle  $\delta_{wall}$ , the value of  $a_{cr,pre}/a_{cr,obs}$  against sliding was nearly 1.4 for all types of retaining walls as shown in Fig. 16.

### Response During Shaking

Fig. 17 shows time histories of input acceleration, displacement of the wall and earth pressure acting on the facing. The wall started to move at about 100 sec on the time scale used in the figure, when the amplitude of the input acceleration was about 100 gal. Since the horizontal displacement at the upper part of the wall (D3) was larger than at its lower part (D1), the major mode of the wall movement before failure was the overturning one, which corresponded to the failure pattern as shown in Photo 1. At almost the same time as above, normal earth pressures acting on the bottom of the base (NLT04-07) started to change gradually. Increase in the normal earth pressure at the toe (NLT07), only small change in the middle (NLT06) and decrease near the heel (NLT05) were consistent with the overturning movement of this wall and with the behavior observed in the tilting test as shown in Fig.13, while the measured earth pressure at the heel (NLT04) in Fig. 17 may have

been incorrect due possibly to breakage in the electric wires. Other normal earth pressures acting on the top of the base (NLT01-03) and on the back of the facing (NFC03 and 08) did not change gradually but showed dynamic fluctuation due to the effect of the cyclic inertia force. Shearing components of the earth pressures did not change gradually except at SLT05 and 07 where large change of normal earth pressures were observed, while their dynamic components were almost the same as or even larger than those for the normal earth pressures. In order to investigate the phase of the dynamic components, enlarged time histories are shown in Fig.18 for the cantilever type wall between 320 and 321 sec corresponding to the amplitude of the input acceleration about 275 gal. Based on this, the phase diagram is schematically shown in Fig. 19. When the horizontal response acceleration of the backfill soil was in the direction opposite to the wall (that is, when the horizontal inertia force is acting toward the facing), normal earth pressures acting on the back of the facing (NFC03 and 08), on the top of the base (NLT01-03) and at the toe of the base (NLT07 and 06) increased, while those near the heel of the base (NLT05) decreased slightly. At this moment, shearing components of the earth pressures increased downwards for the back of the facing (SFC03 and 08), in the direction toward the facing for the top of the base (SLT01-03) and in the opposite direction for the bottom of the base (NLT05-07).

## CONCLUSIONS

The following conclusions can be derived preliminary from the results of tilting and shaking table tests presented in this paper:

1. For tilting tests, the observed and predicted angles of failure plane were almost consistent at  $\delta_{wall}$  between  $1/2\phi - 2/3\phi$ , which was equal to or larger than the mobilized  $\delta_{wall}$  obtained from the analysis of critical tilting angle.
2. For tilting test of cantilever type wall, the measured normal earth pressure at the toe of the wall base got larger than at the heel. This response was consistent with the observed overturning failure, and similar behavior was observed for shaking table test.
3. The observed failure plane for shaking table tests were much steeper than for tilting tests. It may suggest that the seismic behavior assumed in the prediction is not fully correct.
4. For shaking table test of cantilever type wall, gradual change in the earth pressures corresponding to the overturning movement of the wall was observed at the bottom of the base, while dynamic components in the earth pressures were predominant at other locations with their phase relationships as summarized in Fig. 19.

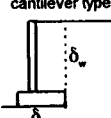
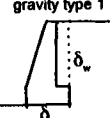
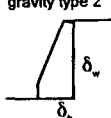
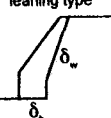
## ACKNOWLEDGMENTS

The authors gratefully acknowledge Prof. Fumio Tatsuoka of the department of Civil Engineering, University of Tokyo for offering thoughtful discussions related to this study, Mr. Hideki Kimura for helping to conduct the tilting tests and Mr. Shinji Ebisawa for assisting to conduct the shaking table tests.

## REFERENCES

1. Tatsuoka, F., Tateyama, M. and Koseki, J.(1996): Performance of Soil Retaining Walls for Railway Embankments, Special Issue of Soils and Foundations on Geotechnical Aspects of the January 17,1995,Hyogoken-Nambu Earthquake, 311-324.
2. Koseki, J., Tateyama, M., Tatsuoka, F., Horii, K.(1996): Back Analyses of Soil Retaining Walls for Railways Embankments Damaged by The 1995 Hyogoken-Nambu Earthquake, The 1995 Hyogoken-Nambu Earthquake -Investigation into Damage to Civil Engineering Structures-, Committee of Earthquake Engineering, Japan Society of Civil Engineers, 101-114
3. Mononobe, N.(1929): On the Determination of Earth Pressures During Earthquakes, Proceeding of World Engineering Congress, Japan
4. Okabe, S.(1924): General Theory on Earth Pressure and Seismic Stability of Retaining Wall and Dam, Journal of Japan Society of Civil Engineers, Vol. 10, 1277-1323
5. Steedman, R. S. and Zeng, X.(1990): The Influence of Phase on the Calculation of Pseudo-Static Earth Pressure on a Retaining Wall, Journal of Geotechnique 40, No.1, 103-112.
6. Richards, R. and Elms, D.G.(1979): Seismic Behavior of Gravity Retaining Walls, Journal of Geotech. Engineering Division, ASCE, Vol.105(4), 449-465.
7. Whitman, R. and Liao, S.(1984): Seismic Design of Gravity Retaining Walls, US Army Eng. Waterways Experiment Sta., Misc. Paper GL-85-1.
8. Yoshida, T.(1995): Strain Localization and Shear Banding During Failure of Sand, Doctoral Thesis, University of Tokyo.

Table 1 Design Parameters

Schematic Diagram of Retaining Walls					
Retaining wall Weight/width (w)	w (gf/cm)	341.06	1390.06 *	1914.56	846.32
Soil properties used to calculate earth pressure	$\gamma$ (gf/cm <sup>3</sup> )	1.62	1.62	1.62	1.62
	c (gf/cm <sup>3</sup> )	0	0	0	0
	$\phi^\circ$	46	46	46	46
	$\delta_w^\circ$	0 - 46	0 - 46	0 - 46	0 - 46
Soil properties used to evaluate stability	$\gamma$ (gf/cm <sup>3</sup> )	1.62	1.62	1.62	1.62
	c (gf/cm <sup>3</sup> )	0	0	0	0
	$\phi^\circ$	46	46	46	46
	$\delta_b^\circ$	46	46	46	46
Surcharge**	q(gf/cm <sup>2</sup> )	32	32	32	32
Surcharge***	q(gf/cm <sup>2</sup> )	10	not performed	10	10

\* for no surcharge w= 883.12 gf/cm

\*\* Tilting Tests

\*\*\* Shaking Table Tests

**Table 2 Prediction of Critical Angle and Observed Failure Pattern for Tilting Tests**

Retaining Wall Type	$\theta_{cr}$ Predicted				Observed Failure Pattern and $\theta_{cr}$
	Sliding		Overturning		
	0	1/2 $\phi$ 2/3 $\phi$ $\phi$	0	1/2 $\phi$ 2/3 $\phi$ $\phi$	
Cantilever <sup>a</sup>	20	25 30 30+	12	16 23 30+	Overturing failure during second tilting, at $\theta_{cr}= 17.1^\circ$
Cantilever <sup>a</sup>	20	25 30 30+	12	16 23 30+	Overturing failure during second tilting, at $\theta_{cr}= 17.6^\circ$
Cantilever <sup>c</sup>	19	23 29 30+	9	14 20 30+	Overturing failure during first tilting, at $\theta_{cr}= 18.3^\circ$
Gravity 1 <sup>a</sup>	19	24 29 30+	12	18 20 30+	Overturing failure during first tilting, at $\theta_{cr}= 18.6^\circ$
Gravity 1 <sup>c</sup>	18	23 28 30+	8	12 15 21	Overturing failure during first tilting, at $\theta_{cr}= 13.2^\circ$
Gravity 2 <sup>c</sup>	18	23 29 30+	9	14 19 30	Overturing failure during first tilting, at $\theta_{cr}= 15.5^\circ$
Leaning <sup>c</sup>	14	18 28 30+	9	13 19 30+	Overturing failure during first tilting, at $\theta_{cr}= 12.2^\circ$

a. no surcharge      b. angle of friction  $\delta_{wall}$       c. with colored sand at the center

**Table 3 Prediction of Critical Acceleration and Observed Failure Pattern for Shaking Table Tests**

Retaining Wall Type	$a_{cr}$ Predicted				Observed Failure Pattern and $a_{cr}$
	Sliding		Overturning		
	0	1/2 $\phi$ 2/3 $\phi$ $\phi$	0	1/2 $\phi$ 2/3 $\phi$ $\phi$	
Cantilever <sup>b</sup>	383	445 554 600+	194	286 424 600+	Overturing failure during shaking, at $a_{cr}= 350$ gal, 5 Hz
Cantilever	383	445 554 600+	194	286 424 600+	Overturing failure during shaking, at $a_{cr}= 375$ gal, 5 Hz
Gravity 2	310	400 550 600+	160	240 400 600+	Overturing failure during shaking, at $a_{cr}= 300$ gal, 5 Hz.
Leaning	250	325 531 600+	158	230 345 600+	Overturing failure during shaking, at $a_{cr}= 250$ gal, 5 Hz
Leaning	250	325 531 600+	158	230 345 600+	Overturing failure during shaking, at $a_{cr}= 250$ gal, 5 Hz
Leaning	250	325 531 600+	158	230 345 600	Overturing failure during shaking, at $a_{cr}= 250$ gal, 5Hz

a. angle of friction  $\delta_{wall}$       b. no surcharge



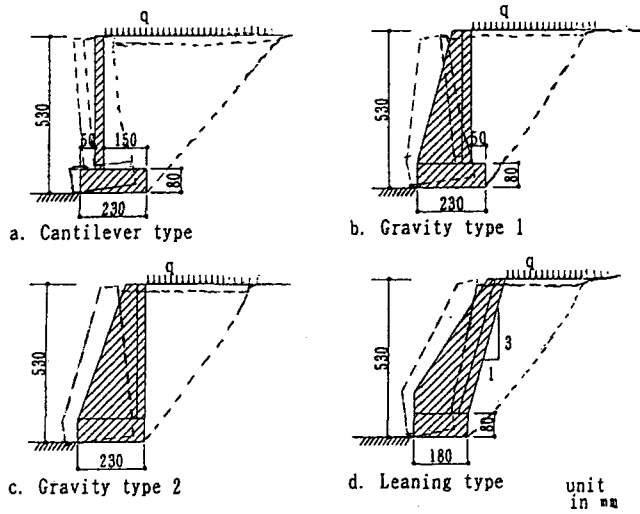


Fig.2 Model of Retaining Walls

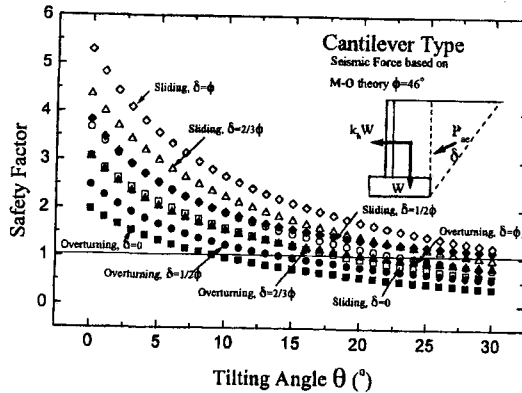


Fig. 3 Predicted Safety Factor Plotted Against Tilting Angle

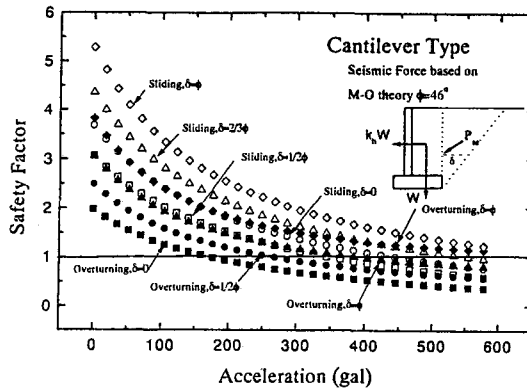


Fig. 4 Predicted Safety Factor Plotted Against Acceleration

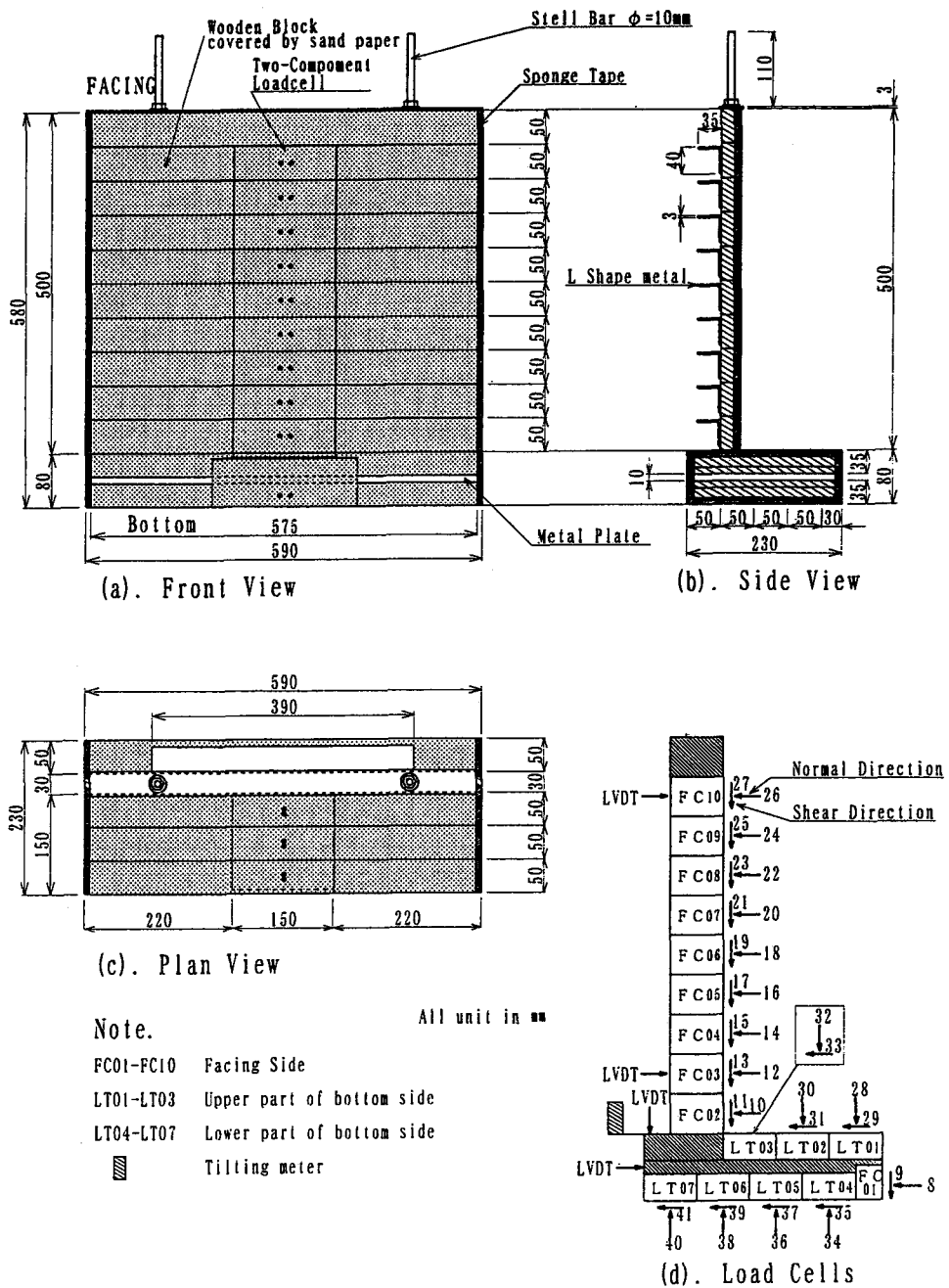
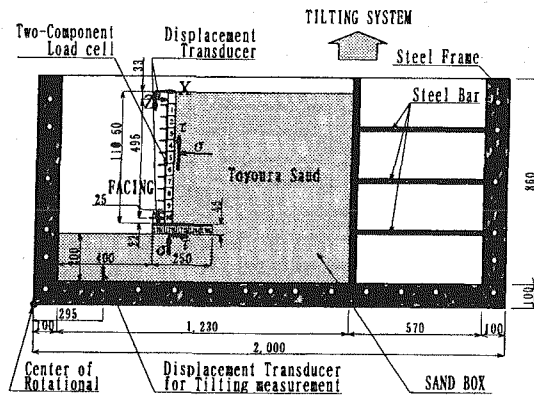
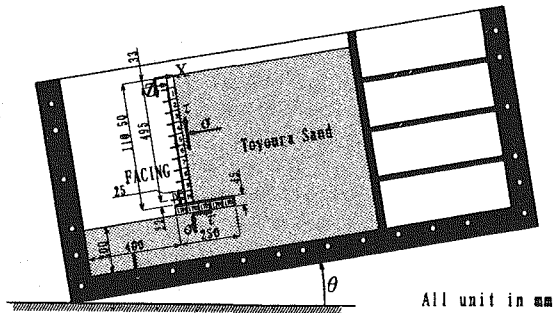


Fig. 5 Model of Wall with Measurement System



(a). After Filling of Sand



(b). During Tilting of Sand Box

Fig. 6 Schematic Diagram for Tilting Tests

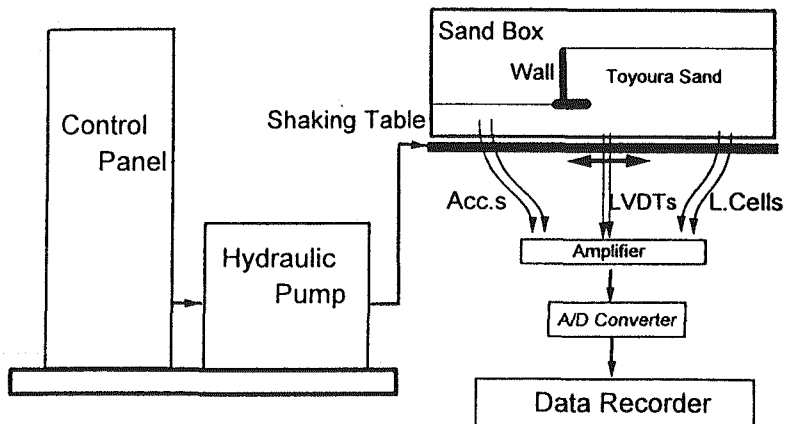


Fig. 7 Schematic Diagram of Experimental set-up

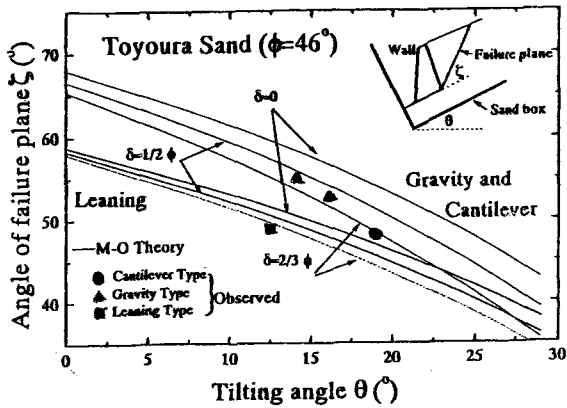


Fig. 8 Angle of Failure Plane ( $\zeta$ ) Plotted Against Tilting Angle( $\theta$ )

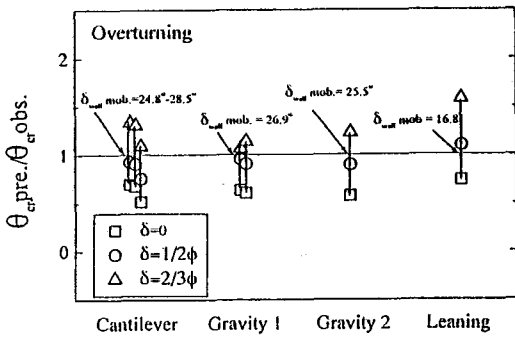


Fig. 9 Ratio of Predicted and Observed Critical Angles

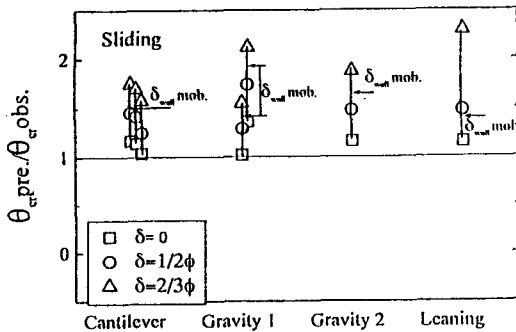


Fig. 10 Ratio of Predicted and Observed Critical Angles

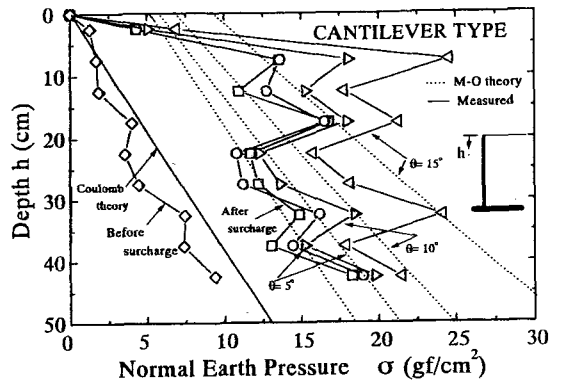


Fig. 11 Normal Earth Pressure Distribution on Backface of Facing During Tilting

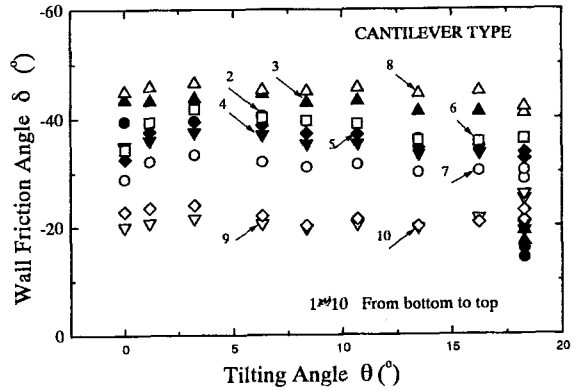


Fig. 12 Wall Friction Angle  $\delta$  During Tilting

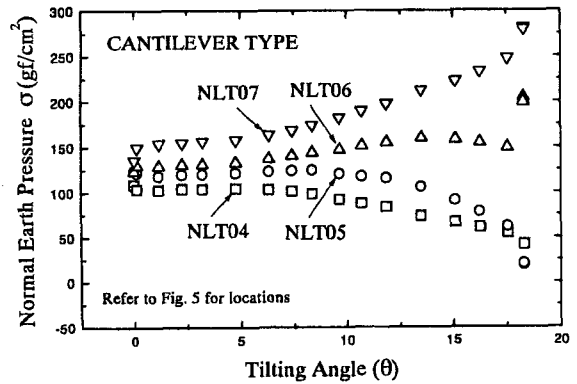
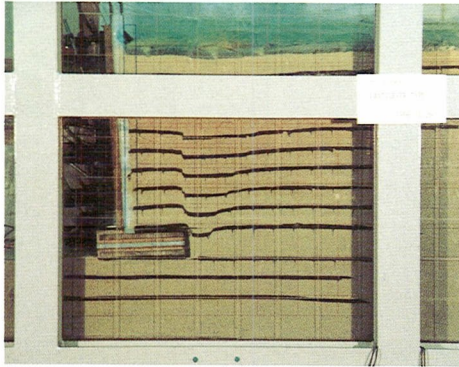


Fig. 13 Normal Earth Pressure Distribution on Bottom of Base During Tilting



Before Shaking



After Shaking

CANTILEVER TYPE

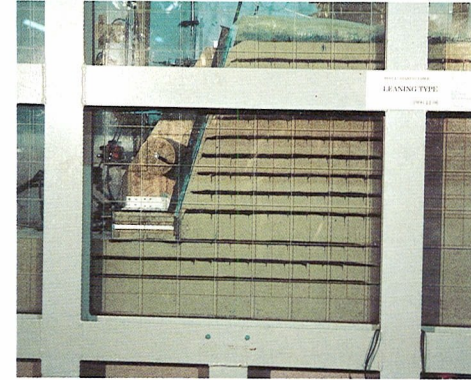


Before Shaking



After Shaking

GRAVITY TYPE



Before Shaking



After Shaking

LEANING TYPE

Photo 1 Typical Observed Failure Plane During Shaking

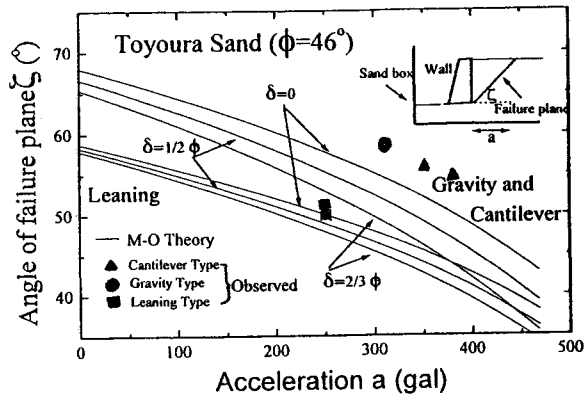


Fig. 14 Angle of Failure Plane  $\zeta$  Plotted Against Acceleration

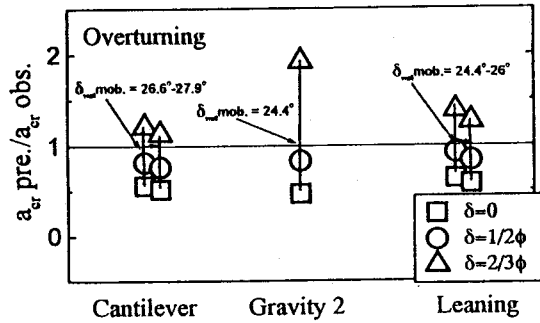


Fig. 15 Ratio of Predicted and Observed Critical Acceleration During Shaking

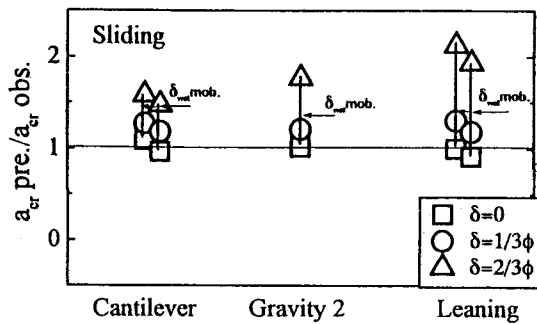


Fig. 16 Ratio of Predicted and Observed Critical Acceleration During Shaking

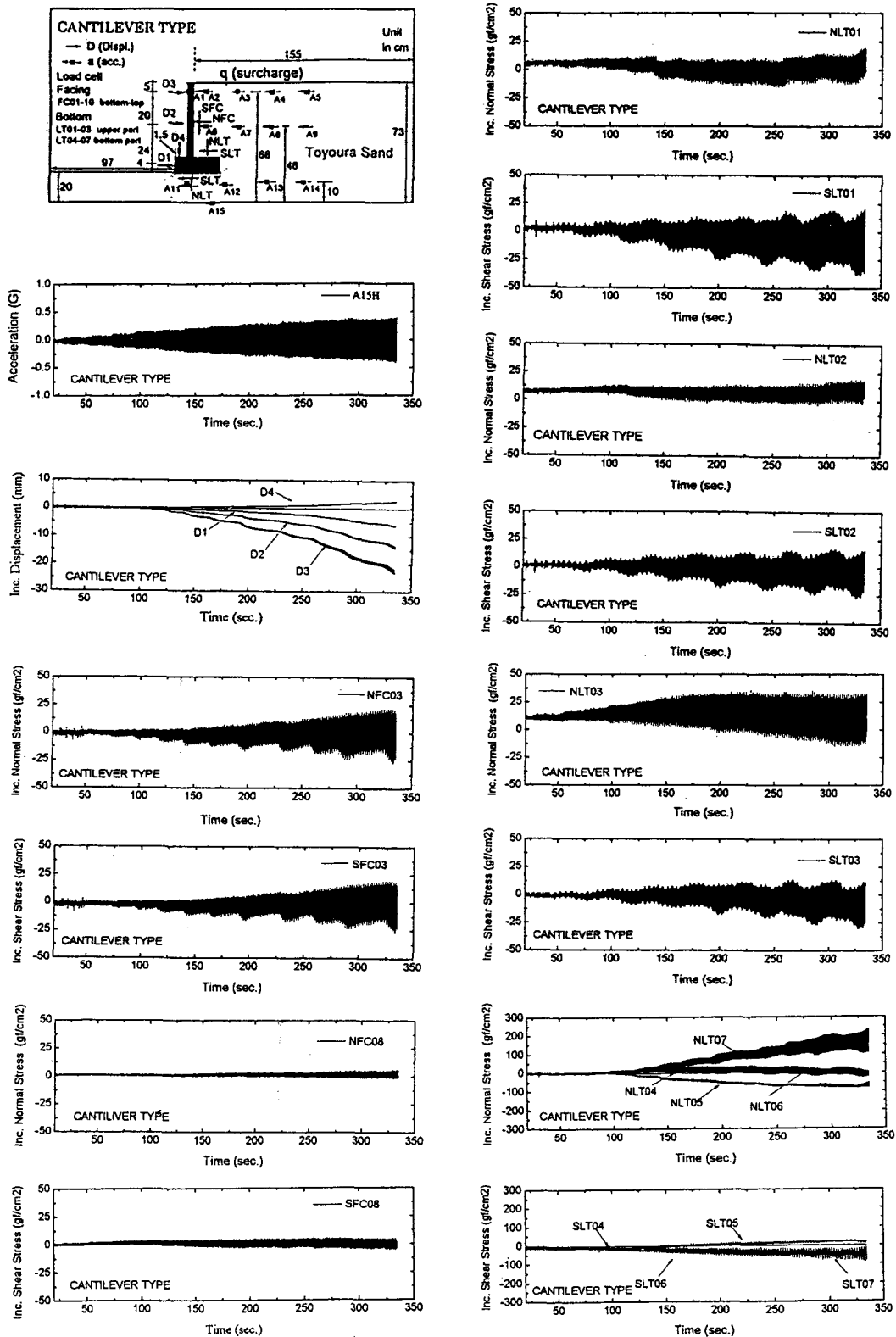


Fig. 17 Time Histories of Horizontal Acceleration, Displacement of Facing and Earth Pressure Acting on the Wall

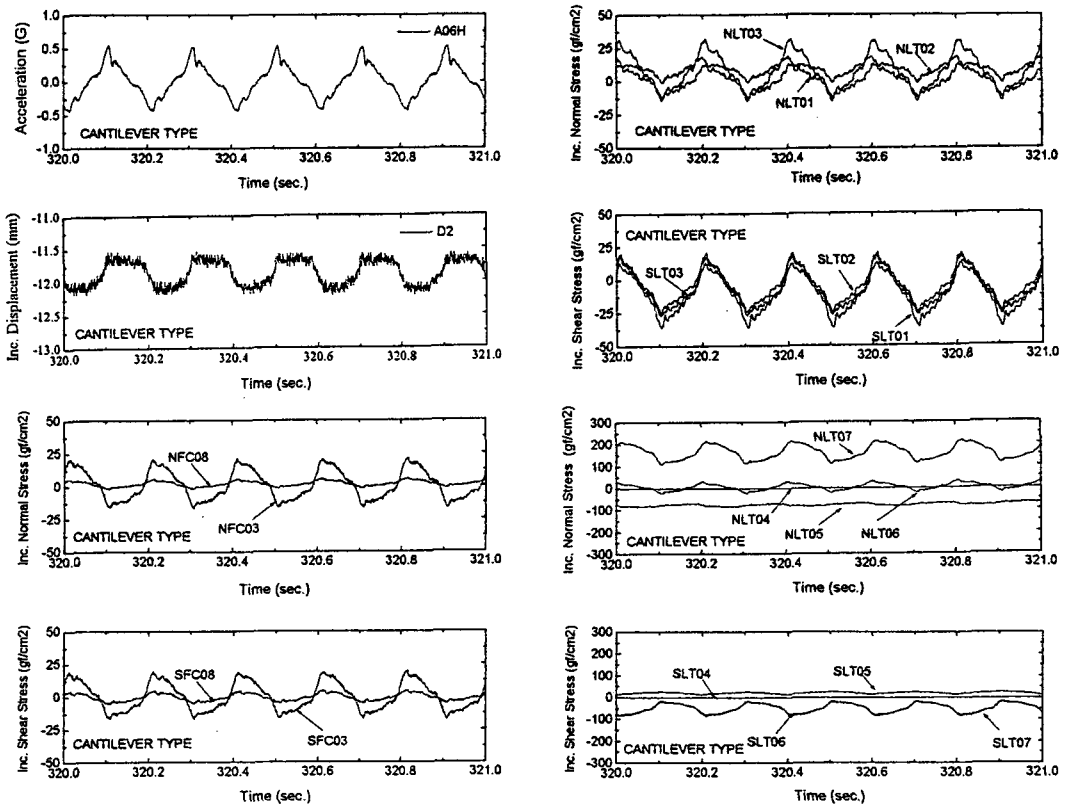


Fig. 18 Phase Diagram for Displacement, Acceleration and Earth Pressure Acting on the Wall

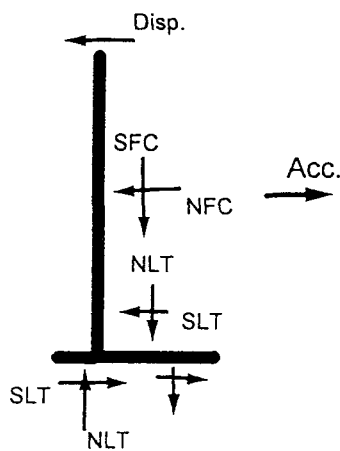


Fig. 19 Direction of Displacement, Acceleration and Earth Pressure Acting on the Wall